3D Printed Polymer Photodetectors

Sung Hyun Park,[‡] Ruitao Su,[‡] Jaewoo Jeong, Shuang-Zhuang Guo, Kaiyan Qiu, Daeha Joung, Fanben Meng, and Michael C. McAlpine*

Extrusion-based 3D printing, an emerging technology, has been previously used in the comprehensive fabrication of light-emitting diodes using various functional inks, without cleanrooms or conventional microfabrication techniques. Here, polymer-based photodetectors exhibiting high performance are fully 3D printed and thoroughly characterized. A semiconducting polymer ink is printed and optimized for the active layer of the photodetector, achieving an external quantum efficiency of 25.3%, which is comparable to that of microfabricated counterparts and yet created solely via a one-pot custom built 3D-printing tool housed under ambient conditions. The devices are integrated into image sensing arrays with high sensitivity and wide field of view, by 3D printing interconnected photodetectors directly on flexible substrates and hemispherical surfaces. This approach is further extended to create integrated multifunctional devices consisting of optically coupled photodetectors and light-emitting diodes, demonstrating for the first time the multifunctional integration of multiple semiconducting device types which are fully 3D printed on a single platform. The 3D-printed optoelectronic devices are made without conventional microfabrication facilities, allowing for flexibility in the design and manufacturing of next-generation wearable and 3D-structured optoelectronics, and validating the potential of 3D printing to achieve high-performance integrated active electronic materials and devices.

3D printing of electronic materials is an emerging fabrication method for devices such as electrodes,[1] batteries,[2] strain sensors,[3,4] capacitors,[5,6] antennas,[7] electrically driven soft actuators,[8] and radio frequency transmitters.[9] These devices have been used in a number of applications including the augmentation of cellular constructs and organ models with electrical components such as sensors and antennas,[10–12] the direct printing of electronic devices on moving surfaces including human hands,[13] and artificial electronic skins.[14–16] Compared with inkjet printing that has been utilized to print optical,[17–19] electrical, and various 3D structures,[20,21] extrusion-based 3D printing is capable of depositing inks with a wider range of viscosities.[22] 3D-printed electronics offer an

interesting alternative over traditional microfabrication technologies for several key reasons, including: 1) the use of low-cost and portable equipment for customizable production; 2) the ability to incorporate both organic/inorganic/biologic and conducting/semiconducting materials using a single printing tool; and 3) the direct fabrication of devices into 3D geometries and onto freeform and even moving surfaces.[13] Indeed, 3D printing has expanded its fabrication capabilities to fully 3D-printed optoelectronic devices such as light-emitting diodes (LEDs), by extruding various functional materials that are first formulated into "inks," enabling the ability to additively construct both planar and 3D optoelectronic architectures.[23]

Photodetectors are an important class of optoelectronic devices and sensors which translate optical information into an electrical readout. Arrays of these devices may be organized into planar configurations, and embedding an array of photodetectors in a cylindrical or hemispherical configuration can yield imaging systems with wide fields of view and minimum image distortions.[24] One approach toward developing imaging systems with nonplanar, curved image sensors is to first fabricate a planar device with thin and deformable materials using microfabrication, and subsequently transfer it to a target surface for a conformal interface.[24–27] In these approaches, the brittleness of the inorganic electronics and inherent planarity of conventional microfabrication methods (e.g., spin-coating, photolithography, and metal deposition) are overcome via a series of novel processing steps, including material thinning and transfer printing for the direct implementation of such devices on curved surfaces. The versatility of 3D printing offers an alternative method to overcome this problem by directly dispensing electronic materials onto any prescribed location on a target surface,[13,14,23] even one that is complex, transforming virtually any surface into a viable platform for semiconducting devices regardless of its shape. In addition, 3D printing could enable the seamless multifunctional integration of various classes of devices on a single platform, enhancing the flexibility for the design and manufacturing of next-generation wearable and 3D-structured optoelectronic devices, and reducing the need for conventional microfabrication.

Here, we report the first fully 3D-printed polymer photodetectors. Our approach involves: 1) demonstrating the printing of functional photodetectors; 2) achieving high performance via

Dr. S. H. Park, R. Su, J. Jeong, Dr. S.-Z. Guo, Dr. K. Qiu, Dr. D. Joung,
Dr. F. Meng, Prof. M. C. McAlpine
Department of Mechanical Engineering
University of Minnesota
Minneapolis, MN 55455, USA
E-mail: mcalpine@umn.edu

The ORCID identification number(s) for the author(s) of this article can be found under https://doi.org/10.1002/adma.201803980.

optimization of the functional inks and the printing process; 3) making use of a diverse set of substrates including flexible plastics and hemispherical glasses; and 4) enabling the integration of devices with different functionalities in a single platform to create multifunctional devices. The printing process involves only four sequential steps to achieve the assorted functional material and device integration. First, we chose the printing substrate with appropriate morphology based on the desired device structure and application. Next, we identified printable materials that have desired functionalities for each component of the devices. Then, to formulate inks from these selected materials, solvents were carefully chosen to ensure the integrity of the structures by improving the uniformity of the material deposition and reducing damage to the underlying layers. Finally, the functional material inks were printed based on pathways dictated by G-code, which was generated via slicing a computer-aided design (CAD) model into multiple layers.

We designed the 3D-printed photodetectors with the following functional materials: 1) a poly(3-hexylthiophene) (P3HT):[6,6]-phenyl C_{61}-butyric acid methyl ester (PCBM) blend as the photoactive layer, 2) poly(ethylenedioxythiophene):polystyrene sulfonate (PEDOT:PSS) as the transparent anode, surrounded by 3) a silver nanoparticle (AgNP) metallic interconnect, with 4) silicone as the electrical insulating layer, and finally, 5) eutectic gallium indium (EGaIn) liquid metal as the cathode as it does not require high-temperature curing (**Figure 1**a). The rheological properties of the inks were characterized (Figure S1, Supporting Information). For solution-based inks with low viscosities, vacuum and pressure were both applied to control the dispensed volume; generally, higher pressure was applied to extrude polymeric inks and the printed pattern was controlled via printing speed and distance between the nozzle and substrate (Table S1, Supporting Information). A schematic of the energy level diagram of the designed structure is shown in Figure 1b (using literature values).[28–36] Upon the reception of incident

photons, charge carriers generated by the electron–hole pairs are separated and transported to the cathode and anode through the PCBM and P3HT phases, respectively. This P3HT:PCBM bulk-heterojunction (BHJ) structure is effective in creating molecular networks that enhance both charge carrier separation and collection efficiencies.[37–40] Based on our measurements (Figure 1c), the P3HT:PCBM layer printed with the blend ink exhibits a broad window of absorption from near-UV (NUV) to visible wavelengths, with the dominant absorption peak at ≈510 nm corresponding to the previously reported P3HT:PCBM blend film with a high degree of ordering.[41]

Each material was printed via the layer-by-layer deposition process on a heat stabilized polyethylene terephthalate (PET) film (Figure 1d). The bilayer of printed AgNPs and PEDOT:PSS replaces the typical transparent conducting oxide electrode, typically an indium tin oxide (ITO) thin film that requires traditional deposition steps such as physical vapor deposition.[42] The printed AgNPs exhibited a uniform thickness of less than 100 nm and consisted of mono- or double layers of particles with diameters smaller than 50 nm (Figure S2, Supporting Information). After annealing at 120 °C for 60 min, the printed AgNP film exhibited a resistivity as low as 8.3×10^{-5} Ω cm, which is within two orders of magnitude of bulk silver. The AgNP ring shape was designed to accept incident light, with the size and shape being adjustable depending on the specific application. In addition, position alignment marks were printed on the substrates with AgNPs to reduce the alignment error of subsequent layer printing (Figure S3, Supporting Information).

Due to the high surface tension of the water-based inks, the printed PEDOT:PSS droplets retained their morphologies on AgNP rings and formed a layer with a low sheet resistance of ≈70 Ω sq^{-1} after curing at 120 °C for 10 min. The P3HT:PCBM inks of various concentrations were printed on the cured PEDOT:PSS to achieve high efficiency. Room temperature
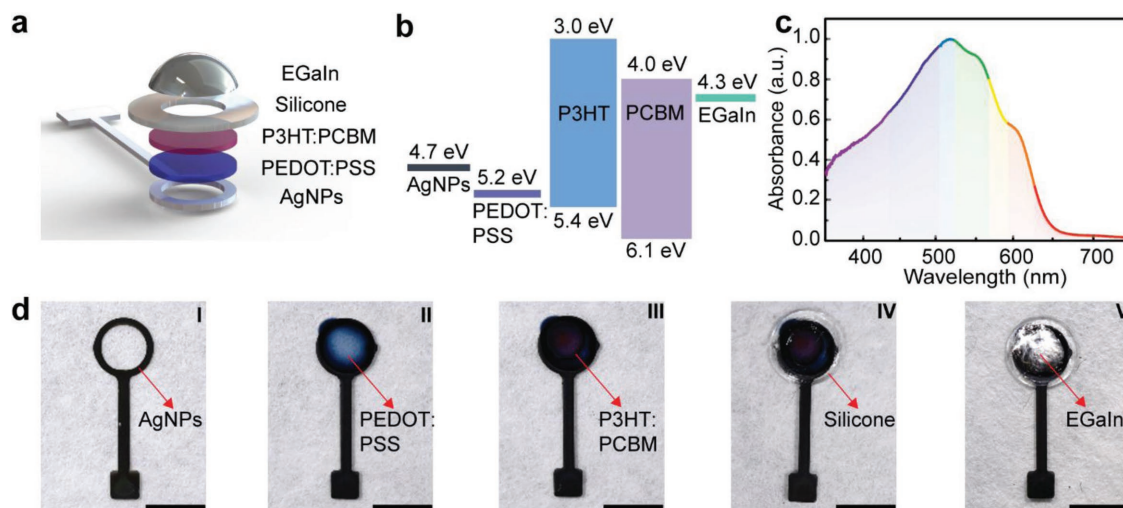

Figure 1. 3D-printed bulk-heterojunction photodetectors. a) Schematic of the structure of the photodetector. b) Energy level diagram showing the work functions and energy gaps of the constitutive layers of the photodetector. c) Normalized NUV–visible absorbance spectra of a 3D-printed P3HT:PCBM layer on a PET film. d) Images showing the steps of 3D printing the photodetector: (I) printing conductive bottom interconnects with AgNPs on PET film; (II) printing the anode material PEDOT:PSS, confined by the boundary of the AgNP pattern; (III) printing a P3HT:PCBM blend on top of PEDOT:PSS; (IV) printing an electrical insulation layer with silicone to separate the bottom conductive layers from the top electrode; and (V) printing EGaIn as the cathode. All scale bars are 4 mm.
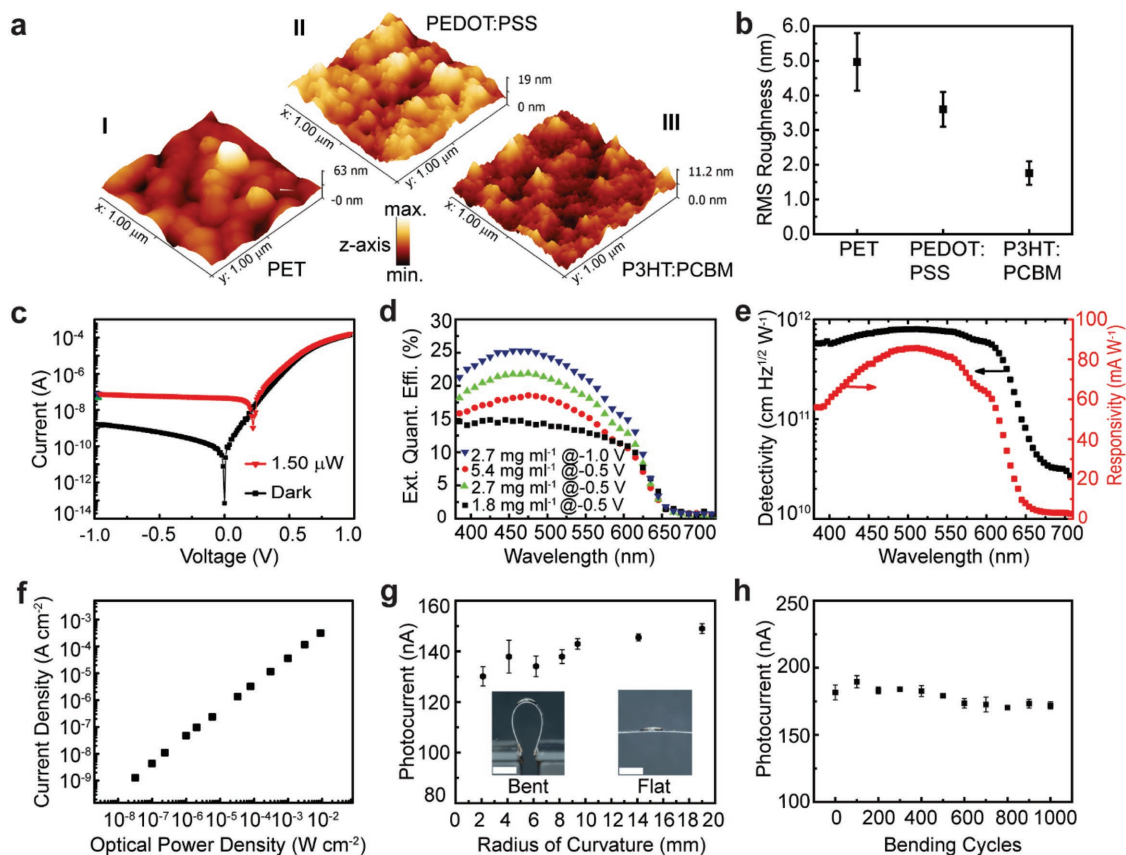
Figure 2. Characterization of 3D-printed photodetectors on PET films. a) Surface morphologies of the 3D-printed polymer layers on a PET substrate. (I) PET substrate; (II) PEDOT:PSS on PET substrate; and (III) P3HT:PCBM on PEDOT:PSS/PET substrate. b) RMS roughness of each printed layer ($N = 7$). c) Current–voltage characteristics of photodetector under dark and 510 nm/1.5 μW illumination. d) EQE of the photodetectors printed with varying P3HT:PCBM ink concentrations. A maximum EQE of 25.3% was achieved with an ink concentration of 2.7 mg mL^{-1} under −1.0 V bias. e) Specific detectivity and responsivity of the 3D-printed photodetector. f) LDR of the 3D-printed photodetector under 510 nm illumination. g) Static bending test of the photodetector, excited by a 650 nm laser with a power of 55 μW ($N = 5$). The insets show the photographs of flat and bent photodetectors. Scale bars are 4 mm. h) Cyclic bending test of the photodetector with a radius of curvature of 6.2 mm, excited by a 650 nm laser with a power of 70 μW ($N = 3$).

vulcanizing (RTV) silicone was then printed to ensure good electrical insulation between the anode and cathode. EGaIn metallic ink was printed as a cathode, eliminating an additional high vacuum metal deposition step and high temperature curing, which would damage the underlying layers. Finally, the printed photodetectors were encapsulated with a UV curable overcoating solution in order to prevent device degradation by oxygen and humidity in the air (Figure S4, Supporting Information).[43,44]

The topography of the printed PEDOT:PSS on PET film and printed P3HT:PCBM on PEDOT:PSS/PET film was characterized by atomic force microscopy (AFM) (**Figure 2**a). The PEDOT:PSS layer with a thickness of ≈300 nm printed on the PET film exhibited a smooth surface with a root mean square (RMS) roughness of 3.6 ± 1.3 nm scanned over a 1 × 1 μm^2 area. The RMS roughness of the P3HT:PCBM layer printed on PEDOT:PSS further decreased to 1.8 ± 0.9 nm (as summarized in Figure 2b), which is comparable to the smoothness of layers deposited by spin-coating methods.[41,45] The printed photodetector exhibited the typical current–voltage (I–V) behavior of a photodiode, showing photogenerated current upon light illumination with a rectification ratio (defined as the

ratio of forward to reverse diode current in the dark at ±1 V) of 10^5, which is comparable to that of microfabrication-based organic photodetectors (Figure 2c).[46,47] Photocurrent generation by the 3D-printed photodetector during a light on/off test can be observed in Movie S1 (Supporting Information).

To evaluate the effect of active material ink concentrations on the external quantum efficiency (EQE) of 3D-printed photodetectors, we prepared the P3HT:PCBM blend ink with a concentration varying from 1.8 to 5.4 mg mL^{-1} to control the thickness of the printed layers (Figure 2d). We found that the ink concentration of 2.7 mg mL^{-1}, corresponding to an effective thickness of ≈50 nm, increased the EQE to 25.3% at −1 V. Further, device operation at −1 V was found to be a reasonable compromise between low dark current and high efficiency, since the photogenerated carrier collection reached a maximum at this reverse bias. The 5.4 mg mL^{-1} solution resulted in a thick active layer (≈155 nm) that lowered the EQE as some photogenerated carriers recombined before reaching the electrodes, which was commonly observed for photodetectors fabricated with low-mobility materials.[45,48–50] The 1.8 mg mL^{-1} solution displayed the lowest EQE due to the thickness nonuniformity of the printed layer, thereby increasing the defect density that

causes the large leakage current.[51] We note that a further increase of EQE is expected with an improvement of the transmittance of the printed PEDOT:PSS layer on a PET film, which is currently between 50% and 70% from NUV to visible wavelength (Figure S5, Supporting Information).

The responsivity (R) and specific detectivity (D^*) of the 3D-printed photodetectors were calculated using the following equations

$$R = \left(J_{ph} - J_d\right)/L(\lambda) \tag{1}$$

$$D^* = RA^{1/2}/\left(2qI_d\right)^{1/2} \tag{2}$$

where J_{ph} is the current density under illumination, J_d is the dark current density, L is the incident light power density at a given wavelength (λ), A is the active area of photodetector, q is the elementary charge, and I_d is the dark current. The maximum responsivity and specific detectivity of the printed photodetector were 86 mA W^{-1} and 8×10^{11} cm $Hz^{1/2}$ W^{-1}, respectively, at $\lambda = 510$ nm (Figure 2e).

Another Figure of merit for photodetectors is the linear dynamic range (LDR), corresponding to the proportionality of the photocurrent with respect to the optical power. The LDR can be expressed as

$$LDR = 20 \log\left(J^*_{ph}/J_d\right) \tag{3}$$

where J^*_{ph} is the current density, measured at a light intensity of 1 mW cm^{-2}.[52] The LDR of the 3D-printed photodetector was ≈80 dB (Figure 2f), which is close to that of a polymer photodetector (100 dB) fabricated by conventional microfabrication methods.[52] The above metrics including EQE, responsivity, specific detectivity and LDR, suggest that fully 3D-printed photodetectors can compete with previously reported ITO-free organic photodetectors fabricated by traditional microfabrication methods.[52–56]

To characterize the flexibility of the printed device, the printed photodetector was mounted on an X–Y–Z micropositioner stage, which allowed the bending radius of the device to be adjusted (Figure 2g). The printed photodetectors showed stable photoresponsive properties without a significant change in the photocurrent generation at a high bending curvature. With decreasing bending radius down to 2.1 mm, the photocurrent was maintained up to 90% of the initial value. This behavior is attributed to the advantageous polymer materials and PET substrate that provided high mechanical flexibility. In addition, the photodetector provided stable photocurrent with minimal variations for 1000 bending cycles (Figure 2h), suggesting that 3D-printed photodetectors may be appropriate for use in flexible and wearable devices.[57–59] The mechanical durability of the stacked layers of the photodetector indicates strong adhesion following thermal annealing.

A critical step is to demonstrate that 3D-printed high-performance photodetectors can be fully integrated into more complex optoelectronic architectures that have potential applications in advanced image sensing technologies (**Figure 3**). First, we demonstrate a fully 3D-printed 5 × 8 photodetector array on a PET substrate (Figure 3a), where photodetectors in

the same row shared a common bottom AgNP interconnect. The diameter of each photodetector and the pixel pitch are 1.6 and 2.5 mm, respectively. All photodetectors in the arrays were fabricated in parallel via the layer-by-layer deposition method (Figure S6, Supporting Information). The printed devices showed high flexibility and good integrity under large bending deformations (Figure 3b). With each photodetector electrically insulated from one another, the detected signals can be retrieved by the address of each pixel. By projecting optical patterns onto the photodetector array and measuring the responsive photocurrent (Figures S7 and S8, Supporting Information), the photodetector array operated effectively as an image sensor that reconstructed the projected patterns (Figure 3c). Notably in Figure 3c, due to the wide LDR of the 3D-printed photodetector, white-light strip patterns with varying intensities were distinguished within the current range of 0–300 nA, which demonstrated the high sensitivity of the image sensor.

Given the inherent capability of 3D printing to build 3D architectures with functional inks, the photodetectors were directly printed onto a hemispherical glass surface (Figure 3d). The CAD model of the concentric AgNP interconnects was designed to conform to the inner surface of the hemispherical dome and further sliced for the generation of G-code instructions (Figure S9, Supporting Information). Then, the subsequent layers were deposited based on the coordinates of each photodetector in 3D space. Due to the surface tension of the inks and adhesion to the substrate, the deposited solutions of the subsequent layers preserved the droplet morphologies and adhered onto the inner surface of the glass hemisphere without migration (Movie S2 and Figures S10 and S11, Supporting Information). I–V sweeps of the printed photodetector on the hemispherical glass corroborated that the performance of the 3D-printed photodetector was not influenced by the curved substrate morphology (Figure 3e). Furthermore, when optical cross mark patterns were projected onto the hemispherical photodetector array, the patterns were successfully reconstructed from two different perspectives (Figure 3f). This result indicated that spherical image sensors can be achieved by the 3D printing, and thus are promising candidates for future bionic eyes.[24,26,27] Because of the rapid prototyping capability of 3D printing, 3D-printed spherical image sensors can be readily customized in terms of photodetector layout and device size in future applications.

High quality, multifunctionally integrated 3D-printed optoelectronic devices demand proper ink selection for each component. For instance, photodetectors and LEDs can be simultaneously printed by replacing the active material with light-emitting polymers. Here, LEDs based on poly[2-methoxy-5-(3′,7′-dimethyloctyloxy)-1,4-phenylenevinylene] (MDMO-PPV) were printed together with P3HT:PCBM-based photodetectors to create one multifunctional optoelectronic device (**Figure 4**a). This device consisted of the following components: 1) three LEDs connected in parallel as the light source; 2) one photodetector in the center as the light detector; and 3) a silver mirror printed on the back side of the substrate to enhance the optical coupling between the LEDs and photodetector (Figure 4b). The full printing process is demonstrated in Movie S3 (Supporting Information), where silver paste was deposited on top of the device to electrically connect the three
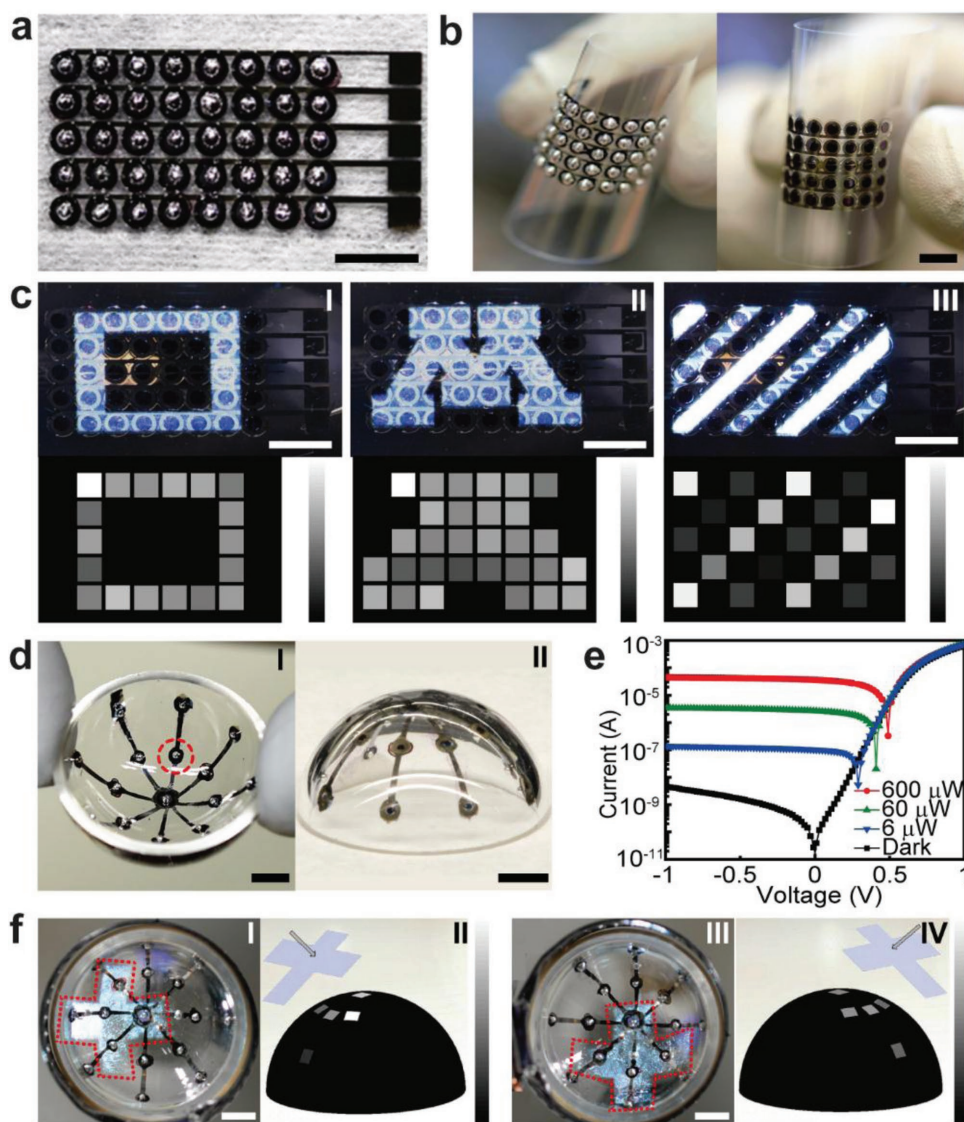
**ADVANCED
SCIENCE NEWS**

www.advancedsciencenews.com

**ADVANCED
MATERIALS**

www.advmat.de

Figure 3. 3D-printed photodetector arrays printed on planar and spherical surfaces. a) 5 × 8 photodetector array printed on PET. b) Photographs of the bent photodetector array on PET films, viewed from both sides. c) Characterization of the flexible photodetector array as an image sensor. Optical patterns projected onto the photodetector array and the reconstructed images: (I) square pattern; (II) letter "M;" and (III) white-light parallel strips with varying intensities. The range of the grayscale bars are from 0 (black) to 300 nA (white). d) Photographs of the concentric photodetector array printed onto the inner surface of a hemispherical glass dome: (I) inside view and (II) outside view of the 3D-printed concentric photodetector array. e) Current–voltage characteristics of the photodetector highlighted in (d). The excitation light source is a 405 nm laser of varying intensities. f) Characterization of the spherical photodetector array as an image sensor. (I) the projected cross mark onto the devices (denoted by the dashed outline); (II) reconstructed cross mark pattern; (III and IV) cross mark pattern projected onto the spherical photodetector array rotated 90° and the reconstructed cross mark pattern. The range of the grayscale bar is from 0 (black) to 300 nA (white). Scale bars are 5 mm.

LEDs and create cathode leads for both the LEDs and the photodetector. The silver paste was room-temperature curable, which prevented degradation of the active layers during thermal annealing. The emission spectrum of MDMO-PPV-based LEDs covered the spectral range of 500–700 nm with a peak at 586 nm (Figure 4c). The LEDs adopted a similar layer-by-layer structure, where the light was extracted through the annular AgNP ring at the bottom of the stack. Figure 4d shows the I–V characteristic of the 3D-printed LED with a turn-on voltage of ≈2 V, and the inset images display the on/off states of the three LEDs.

In this side-by-side layout of a multifunctional device, coupling between devices was manifested via photocurrent generation in the photodetector upon detection of the light reflected off of the backside printed silver mirror. To first verify the photocurrent response of the photodetector as a module in the multifunctional device, an incident pulse illumination of λ = 510 nm and 1.5 µW was directly applied to the photodetector. A response magnitude of 60 nA was observed under −1 V bias (Figure 4e). Then, a pulse signal of 0.8 Hz at 10 V was applied to the three LEDs in parallel to generate light for the excitation of the photodetector (Movie S4, Supporting Information).
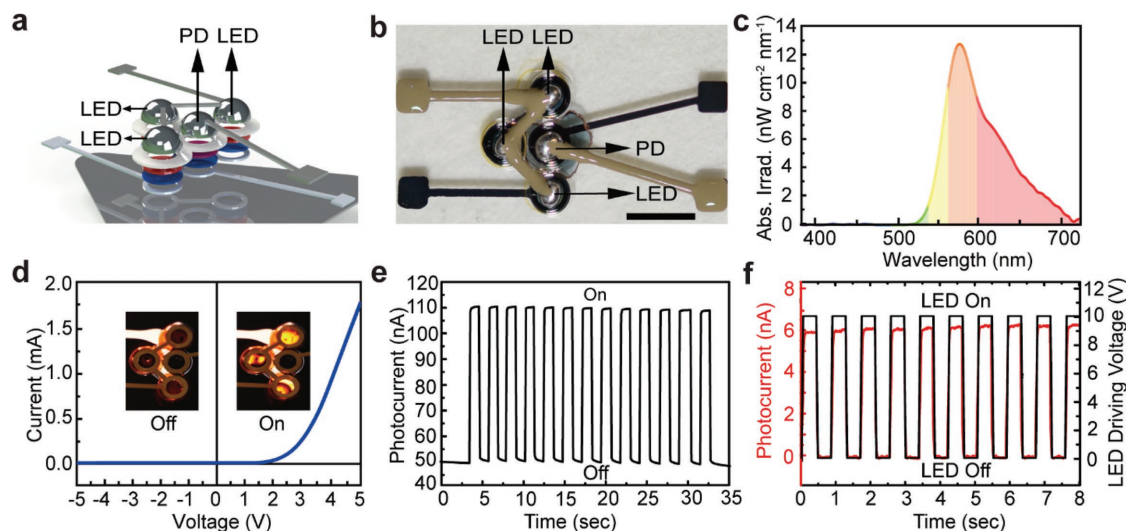
Figure 4. 3D-printed photodetector–LED multifunctional device. a) Schematic showing the configuration of the multifunctional device. b) Photograph of the 3D-printed photodetector–LED multifunctional device. The 3D-printed bottom silver mirror was excluded for device image clarity. Scale bar is 5 mm. c) Electroluminescence of the 3D-printed LED with MDMO-PPV as the emissive material. d) Current–voltage characteristic of the 3D-printed LED. Insets show the turn-on and turn-off states of the three LEDs connected in parallel. e) Photocurrent measurement of the 3D-printed photodetector as the sensor of a multifunctional device under a pulsed light illumination. The applied bias is −1 V and the wavelength of the light source is 510 nm with a power of 1.5 µW. f) Photocurrent response of the photodetector measured under a pulse bias applied to the LEDs.

Photocurrent response of the same frequency was measured by the photodetector (Figure 4f), demonstrating successful operation of the multifunctional optoelectronic device. With the recent demonstration of directly printing functional materials on the human body for biometric sensing,[13,14] this hybrid optoelectronic configuration could ultimately be directly printed on the skin for wearable optoelectronics. Compared with microfabricated inorganic and organic multifunctional optoelectronic devices,[27,60] 3D-printed optoelectronics offer an attractive alternative in terms of device layout design, simplified procedures for fabrication, and portability of the instrumentation.

In summary, we have designed and fully 3D-printed polymer photodetectors. Individual devices exhibited high performance, validating the potential of a fully 3D-printed device. By tuning the concentrations of the inks which comprise the active layers, the thicknesses and uniformities were optimized to achieve high EQE and specific detectivity, comparable to those of spin-coated devices. Interconnected photodetector arrays and integrated multifunctional devices were achieved via the same one-pot platform. These arrays printed on both planar and hemispherical surfaces showed high sensitivity and wide field-of-view, demonstrating promising applications as advanced image sensors. Further, we expanded from homogeneous device arrays to multifunctional devices by directly printing optically coupled photodetectors and LEDs on a single platform.

Future studies will focus on the following: 1) further improving the performance of the 3D-printed photodetectors to match those of commercial photodetectors; 2) improving the image sensing resolution by scaling down the feature sizes of the photodetectors; 3) further developing the 3D-printed spherical image sensors into "bionic eye" vision systems; 4) fully 3D printing all-in-one multifunctional devices that integrate onboard power options; and 5) implementing adaptive printing of the multifunctional device on the human body, for example, as a customizable optical sensor

that monitors physiological metrics such as pulse rate and blood oxygen. Overall, extrusion-based 3D printing of optoelectronic devices offers a novel route for the "facility-free" fabrication of 3D-structured photonics and wearable sensors.

Experimental Section

Ink Preparation: A P3HT:PCBM blend solution was prepared by mixing P3HT (MilliporeSigma, Inc.) chlorobenzene solution (30 mg mL⁻¹) and PCBM (MilliporeSigma, Inc.) chlorobenzene solution (24 mg mL⁻¹). The mixture was then stirred at 700 rpm for 24 h. The solution was diluted to 1/5, 1/10, and 1/15 of the initial concentration for the device fabrication. MDMO-PPV (MilliporeSigma, Inc.) toluene solution (1.6 mg mL⁻¹) was prepared by stirring at 700 rpm for 24 h. All other inks were used as received from the vendors without further modification.

Device Fabrication: To clean the substrates, PET film (MELINEX ST505, Tekra) and a hemispherical glass dome (1 in. diameter, Chemglass, Inc.) were sonicated in isopropanol and rinsed in deionized water. The cleaned substrates were dried by blowing with N₂. AgNPs with a concentration of 35 wt% (MilliporeSigma, Inc.) were then printed on the substrate. PEDOT:PSS (MilliporeSigma, Inc.) solution was sonicated and filtered with a 450 nm polyvinylidene fluoride (PVDF) filter before printing. Active inks including P3HT:PCBM for the photodetector and MDMO-PPV for the LED were filtered with a 450 nm polytetrafluoroethylene (PTFE) filter before printing. The insulating layer was printed with a room temperature vulcanizing silicone (Loctite, Henkel, Co.). EGaIn (MilliporeSigma, Inc.) was printed as the cathode material. For the multifunctional device, silver paste (MiliporeSigma, Inc.) was printed to connect the individual photodetectors. Finally, UV curable resin (Novacentrix, Inc.) was printed to encapsulate the device. Optoelectronic devices were printed via a motion-executing system (AGS1000 Gantry System, Aerotech, Inc.), with the inks dispensed by a pressure regulator (Ultimus V Dispenser, Nordson EFD, Co.). Detailed parameters for material printing conditions are displayed in Table S1 (Supporting Information).

Single Device Characterization: Surface morphologies of different layers were characterized by AFM (Agilent 5500, Keysight Technologies, Inc.). For the measurement of I–V data, EQE, specific detectivity, responsivity,

**ADVANCED
SCIENCE NEWS**
www.advancedsciencenews.com

**ADVANCED
MATERIALS**
www.advmat.de

and LDR, a Xenon short arc lamp (Ushino, UXL-75 XE) was employed as the light source. The photodetector was excited by monochromatic light that was directed through an optical fiber (QP1000-2-UV-VIS, Ocean Optics, Inc.) from a holographic grating monochromator (Cornerstone 130-RG-1-MC, Newport, Co.). The Xenon short arc lamp and monochromator were calibrated with the photodiode power sensor (S130VC, Thorlabs, Inc.) and spectrometer (FLAME-S-VIS-NIR-ES, Ocean Optics, Inc.) to adjust wavelength and light intensity. The generated photocurrent was measured by a source-meter unit (Keithley 2450, Tektronix, Inc.). For the static bending test, one single photodetector was suspended between an X–Y–Z translational stage and the horizontal moving stage of the 3D printer. A 650 nm laser with ND filters was used as the light source for static (55 µW) and cyclic (70 µW) tests. The emission spectrum of the MDMO-PPV LED was measured by pointing the cosine corrector (CC-3-UV-S, Ocean Optics, Inc.) to the bottom of the device and connecting to the spectrometer.

Photodetector Array Characterization: Both planar and spherical photodetector arrays were mounted onto self-built holders and connected to the source-meter unit (Keithley 2450, Tektronix, Inc.) via two probes (Cascade Microtech, Inc.). During the tests, various optical patterns were projected onto the photodetector array to illuminate the selected pixels by a projector (DSV0920, Acer, Inc.) under ambient conditions.

Supporting Information

Supporting Information is available from the Wiley Online Library or from the author.

Conflict of Interest

The corresponding author (M. C. McAlpine) is co-inventor on a (currently unlicensed) patent involving 3D printing active electronic materials and devices: https://patents.google.com/patent/US9887356B2.

[1] A. J. Lopes, E. MacDonald, R. B. Wicker, *Rapid Prototyping J.* **2012**, *18*, 129.
[2] K. Sun, T. S. Wei, B. Y. Ahn, J. Y. Seo, S. J. Dillon, J. A. Lewis, *Adv. Mater.* **2013**, *25*, 4539.
[3] J. T. Muth, D. M. Vogt, R. L. Truby, Y. Mengüç, D. B. Kolesky, R. J. Wood, J. A. Lewis, *Adv. Mater.* **2014**, *26*, 6307.
[4] S. Sundaram, Z. Jiang, P. Sitthi-Amorn, D. S. Kim, M. A. Baldo, W. Matusik, *Adv. Mater. Technol.* **2017**, *2*, 1600257.
[5] C. Zhao, C. Y. Wang, R. Gorkin, S. Beirne, K. W. Shu, G. G. Wallace, *Electrochem. Commun.* **2014**, *41*, 20.
[6] C. Zhu, T. Liu, F. Qian, T. Y.-J. Han, E. B. Duoss, J. D. Kuntz, C. M. Spadaccini, M. A. Worsley, Y. Li, *Nano Lett.* **2016**, *16*, 3448.
[7] J. J. Adams, E. B. Duoss, T. F. Malkowski, M. J. Motala, B. Y. Ahn, R. G. Nuzzo, J. T. Bernhard, J. A. Lewis, *Adv. Mater.* **2011**, *23*, 1335.
[8] G. Haghiashtiani, E. Habtour, S. H. Park, F. Gardea, M. C. McAlpine, *Extreme Mech. Lett.* **2018**, *21*, 1.
[9] N. Zhou, C. Liu, J. A. Lewis, D. Ham, *Adv. Mater.* **2017**, *29*, 1605198.
[10] M. S. Mannoor, Z. Jiang, T. James, Y. L. Kong, K. A. Malatesta, W. O. Soboyejo, N. Verma, D. H. Gracias, M. C. McAlpine, *Nano Lett.* **2013**, *13*, 2634.
[11] K. Qiu, Z. Zhao, G. Haghiashtiani, S. Z. Guo, M. He, R. Su, Z. Zhu, D. B. Bhuiyan, P. Murugan, F. Meng, S. H. Park, C. C. Chu, B. M. Ogle, D. A. Saltzman, B. R. Konety, R. M. Sweet, M. C. McAlpine, *Adv. Mater. Technol.* **2018**, *3*, 1700235.
[12] K. Qiu, G. Haghiashtiani, M. C. McAlpine, *Annu. Rev. Anal. Chem.* **2018**, *11*, 287.
[13] Z. Zhu, S. Z. Guo, T. Hirdler, C. Eide, X. Fan, J. Tolar, M. C. McAlpine, *Adv. Mater.* **2018**, *30*, 1707495.
[14] S. Z. Guo, K. Qiu, F. Meng, S. H. Park, M. C. McAlpine, *Adv. Mater.* **2017**, *29*, 1701218.
[15] A. D. Valentine, T. A. Busbee, J. W. Boley, J. R. Raney, A. Chortos, A. Kotikian, J. D. Berrigan, M. F. Durstock, J. A. Lewis, *Adv. Mater.* **2017**, *29*, 1703817.
[16] R. L. Truby, M. Wehner, A. K. Grosskopf, D. M. Vogt, S. G. M. Uzel, R. J. Wood, J. A. Lewis, *Adv. Mater.* **2018**, *30*, 1706383.
[17] L. Wu, Z. Dong, F. Li, H. Zhou, Y. Song, *Adv. Opt. Mater.* **2016**, *4*, 1915.
[18] Z. Gu, Z. Huang, C. Li, M. Li, Y. Song, *Sci. Adv.* **2018**, *4*, eaat2390.
[19] Z. Gu, K. Wang, H. Li, M. Gao, L. Li, M. Kuang, Y. S. Zhao, M. Li, Y. Song, *Small* **2017**, *13*, 1603217.
[20] W. Li, F. Li, H. Li, M. Su, M. Gao, Y. Li, D. Su, X. Zhang, Y. Song, *ACS Appl. Mater. Interfaces* **2016**, *8*, 12369.
[21] L. Wu, Z. Dong, M. Kuang, Y. Li, F. Li, L. Jiang, Y. Song, *Adv. Funct. Mater.* **2015**, *25*, 2237.
[22] Y. Zhang, F. Zhang, Z. Yan, Q. Ma, X. Li, Y. Huang, J. A. Rogers, *Nat. Rev. Mater.* **2017**, *2*, 17019.
[23] Y. L. Kong, I. A. Tamargo, H. Kim, B. N. Johnson, M. K. Gupta, T.-W. Koh, H.-A. Chin, D. A. Steingart, B. P. Rand, M. C. McAlpine, *Nano Lett.* **2014**, *14*, 7017.
[24] Y. M. Song, Y. Xie, V. Malyarchuk, J. Xiao, I. Jung, K.-J. Choi, Z. Liu, H. Park, C. Lu, R.-H. Kim, R. Li, K. B. Crozier, Y. Huang, J. A. Rogers, *Nature* **2013**, *497*, 95.
[25] B. Guenter, N. Joshi, R. Stoakley, A. Keefe, K. Geary, R. Freeman, J. Hundley, P. Patterson, D. Hammon, G. Herrera, E. Sherman, A. Nowak, R. Schubert, P. Brewer, L. Yang, R. Mott, G. McKnight, *Opt. Express* **2017**, *25*, 13010.
[26] K. Zhang, Y. H. Jung, S. Mikael, J. H. Seo, M. Kim, H. Y. Mi, H. Zhou, Z. Y. Xia, W. D. Zhou, S. Q. Gong, Z. Q. Ma, *Nat. Commun.* **2017**, *8*, 1782.
[27] C. Choi, M. K. Choi, S. Y. Liu, M. S. Kim, O. K. Park, C. Im, J. Kim, X. L. Qin, G. J. Lee, K. W. Cho, M. Kim, E. Joh, J. Lee, D. Son, S. H. Kwon, N. L. Jeon, Y. M. Song, N. S. Lu, D. H. Kim, *Nat. Commun.* **2017**, *8*, 1664.
[28] S. Narioka, H. Ishii, D. Yoshimura, M. Sei, Y. Ouchi, K. Seki, S. Hasegawa, T. Miyazaki, Y. Harima, K. Yamashita, *Appl. Phys. Lett.* **1995**, *67*, 1899.
[29] J. Huang, P. F. Miller, J. S. Wilson, A. J. de Mello, J. C. de Mello, D. D. C. Bradley, *Adv. Funct. Mater.* **2005**, *15*, 290.

[30] M. S. White, D. C. Olson, S. E. Shaheen, N. Kopidakis, D. S. Ginley, *Appl. Phys. Lett.* **2006**, *89*, 143517.

[31] R. C. Chiechi, E. A. Weiss, M. D. Dickey, G. M. Whitesides, *Angew. Chem., Int. Ed.* **2008**, *47*, 142.

[32] H. Kim, M. Shin, Y. Kim, *EPL* **2008**, *84*, 58002.

[33] Z.-L. Guan, J. B. Kim, H. Wang, C. Jaye, D. A. Fischer, Y.-L. Loo, A. Kahn, *Org. Electron.* **2010**, *11*, 1779.

[34] D. J. Lipomi, B. C. K. Tee, M. Vosgueritchian, Z. Bao, *Adv. Mater.* **2011**, *23*, 1771.

[35] K.-Y. Cheng, R. Anthony, U. R. Kortshagen, R. J. Holmes, *Nano Lett.* **2011**, *11*, 1952.

[36] P.-Q. Bi, B. Wu, F. Zheng, W.-L. Xu, X.-Y. Yang, L. Feng, F. Zhu, X.-T. Hao, *ACS Appl. Mater. Interfaces* **2016**, *8*, 23212.

[37] G. Yu, J. Gao, J. C. Hummelen, F. Wudl, A. J. Heeger, *Science* **1995**, *270*, 1789.

[38] G. Yu, A. J. Heeger, *J. Appl. Phys.* **1995**, *78*, 4510.

[39] J. J. M. Halls, C. A. Walsh, N. C. Greenham, E. A. Marseglia, R. H. Friend, S. C. Moratti, A. B. Holmes, *Nature* **1995**, *376*, 498.

[40] G. Li, R. Zhu, Y. Yang, *Nat. Photonics* **2012**, *6*, 153.

[41] G. Li, V. Shrotriya, J. Huang, Y. Yao, T. Moriarty, K. Emery, Y. Yang, *Nat. Mater.* **2005**, *4*, 864.

[42] A. L. Dawar, J. C. Joshi, *J. Mater. Sci.* **1984**, *19*, 1.

[43] V. N. Savvate'ev, A. V. Yakimov, D. Davidov, R. M. Pogreb, R. Neumann, Y. Avny, *Appl. Phys. Lett.* **1997**, *71*, 3344.

[44] J. Lewis, *Mater. Today* **2006**, *9*, 38.

[45] S. S. van Bavel, M. Bärenklau, G. de With, H. Hoppe, J. Loos, *Adv. Funct. Mater.* **2010**, *20*, 1458.

[46] B. Luszczynska, M. Z. Szymanski, J. M. Verilhac, P. Reiss, D. Djurado, *Org. Electron.* **2013**, *14*, 3206.

[47] L. Zhang, T. Yang, L. Shen, Y. Fang, L. Dang, N. Zhou, X. Guo, Z. Hong, Y. Yang, H. Wu, J. Huang, Y. Liang, *Adv. Mater.* **2015**, *27*, 6496.

[48] M. Stolterfoht, A. Armin, B. Philippa, R. D. White, P. L. Burn, P. Meredith, G. Juska, A. Pivrikas, *Sci. Rep.* **2015**, *5*, 9949.

[49] S. van Bavel, E. Sourty, G. de With, K. Frolic, J. Loos, *Macromolecules* **2009**, *42*, 7396.

[50] M. Ramuz, L. Bürgi, C. Winnewisser, P. Seitz, *Org. Electron.* **2008**, *9*, 369.

[51] M. S. White, M. Kaltenbrunner, E. D. Glowacki, K. Gutnichenko, G. Kettlgruber, I. Graz, S. Aazou, C. Ulbricht, D. A. M. Egbe, M. C. Miron, Z. Major, M. C. Scharber, T. Sekitani, T. Someya, S. Bauer, N. S. Sariciftci, *Nat. Photonics* **2013**, *7*, 811.

[52] X. Gong, M. Tong, Y. Xia, W. Cai, J. S. Moon, Y. Cao, G. Yu, C.-L. Shieh, B. Nilsson, A. J. Heeger, *Science* **2009**, *325*, 1665.

[53] J. Huang, X. Wang, Y. Kim, A. J. deMello, D. D. C. Bradley, J. C. Demello, *Phys. Chem. Chem. Phys.* **2006**, *8*, 3904.

[54] D. Baierl, B. Fabel, P. Lugli, G. Scarpa, *Org. Electron.* **2011**, *12*, 1669.

[55] B. Arredondo, C. de Dios, R. Vergaz, A. R. Criado, B. Romero, B. Zimmermann, U. Würfel, *Org. Electron.* **2013**, *14*, 2484.

[56] C. M. Benavides, P. Murto, C. L. Chochos, V. G. Gregoriou, A. Avgeropoulos, X. Xu, K. Bini, A. Sharma, M. R. Andersson, O. Schmidt, C. J. Brabec, E. Wang, S. F. Tedde, *ACS Appl. Mater. Interfaces* **2018**, *10*, 12937.

[57] V. T. Tran, Y. F. Wei, H. Y. Yang, Z. Y. Zhan, H. J. Du, *Nanotechnology* **2017**, *28*, 095204.

[58] Y. H. Dong, Y. S. Zou, J. Z. Song, J. H. Li, B. N. Han, Q. S. Shan, L. M. Xu, J. Xue, H. B. Zeng, *Nanoscale* **2017**, *9*, 8580.

[59] Q. Shuang, L. Jihong, N. Xiaona, L. Baolai, F. Guangsheng, L. Zhiqiang, W. Shufang, P. Kailiang, P. Caofeng, *Adv. Funct. Mater.* **2018**, *28*, 1707311.

[60] C. M. Lochner, Y. Khan, A. Pierre, A. C. Arias, *Nat. Commun.* **2014**, *5*, 5745.